







# The Kinetics of SARS-CoV-2 Antibody Development Is Associated with Clearance of RNAemia

Chuangqi Wang,<sup>a</sup> Yijia Li,<sup>b,c</sup> Paulina Kaplonek,<sup>d</sup> Matteo Gentili,<sup>e</sup> Stephanie Fischinger,<sup>d</sup> Kathryn A. Bowman,<sup>b,c,d</sup> Moshe Sade-Feldman,<sup>e</sup> Kyle R. Kays,<sup>c</sup> James Regan,<sup>b</sup> James P. Flynn,<sup>b</sup> Marcia B. Goldberg,<sup>c,e,f</sup>  Nir Hacohen,<sup>e</sup>  Michael R. Filbin,<sup>b,e</sup>  Douglas A. Lauffenburger,<sup>a</sup>  Galit Alter,<sup>c,d</sup> Jonathan Z. Li<sup>b</sup>

<sup>a</sup>Department of Biological Engineering, Massachusetts Institute of Technology, Cambridge, Massachusetts, USA

<sup>b</sup>Brigham and Women's Hospital, Boston, Massachusetts, USA

<sup>c</sup>Massachusetts General Hospital, Boston, Massachusetts, USA

<sup>d</sup>Ragon Institute of MGH, MIT and Harvard, Cambridge, Massachusetts, USA

<sup>e</sup>Broad Institute of MIT and Harvard, Cambridge, Massachusetts, USA

<sup>f</sup>Department of Microbiology, Harvard Medical School, Boston, Massachusetts, USA

Chuangqi Wang, Yijia Li, and Paulina Kaplonek, Galit Alter, and Jonathan Z. Li contributed equally. Author order was determined by their contribution to this paper.

**ABSTRACT** Persistent SARS-CoV-2 replication and systemic dissemination are linked to increased COVID-19 disease severity and mortality. However, the precise immune profiles that track with enhanced viral clearance, particularly from systemic RNAemia, remain incompletely defined. To define whether antibody characteristics, specificities, or functions that emerge during natural infection are linked to accelerated containment of viral replication, we examined the relationship of SARS-CoV-2-specific humoral immune evolution in the setting of SARS-CoV-2 plasma RNAemia, which is tightly associated with disease severity and death. On presentation to the emergency department, S-specific IgG3, IgA1, and Fc $\gamma$ -receptor (Fc $\gamma$ R) binding antibodies were all inversely associated with higher baseline plasma RNAemia. Importantly, the rapid development of spike (S) and its subunit (S1/S2/receptor binding domain)-specific IgG, especially Fc $\gamma$ R binding activity, were associated with clearance of RNAemia. These results point to a potentially critical and direct role for SARS-CoV-2-specific humoral immune clearance on viral dissemination, persistence, and disease outcome, providing novel insights for the development of more effective therapeutics to resolve COVID-19.

**IMPORTANCE** We showed that persistent SARS-CoV-2 RNAemia is an independent predictor of severe COVID-19. We observed that SARS-CoV-2-targeted antibody maturation, specifically Fc-effector functions rather than neutralization, was strongly linked with the ability to rapidly clear viremia. This highlights the critical role of key humoral features in preventing viral dissemination or accelerating viremia clearance and provides insights for the design of next-generation monoclonal therapeutics. The main key points will be that (i) persistent SARS-CoV-2 plasma RNAemia independently predicts severe COVID-19 and (ii) specific humoral immune functions play a critical role in halting viral dissemination and controlling COVID-19 disease progression.

**KEYWORDS** longitudinal data modeling, persistent SARS-CoV-2 plasma viremia, system serology, viremia, humoral immune response

Accumulating evidence has shown that SARS-CoV-2 systemic dissemination, as manifested by levels of plasma RNAemia, is linked to more extensive tissue damage, endothelial inflammation, and coagulopathies and predicts the risk of eventual disease severity and death (1–3). In immunosuppressed individuals, persistent SARS-CoV-2 RNAemia has also been detected and is thought to play a role in disease

**Editor** Diane E. Griffin, Johns Hopkins Bloomberg School of Public Health

**Copyright** © 2022 Wang et al. This is an open-access article distributed under the terms of the [Creative Commons Attribution 4.0 International license](https://creativecommons.org/licenses/by/4.0/).

Address correspondence to Jonathan Z. Li, [jlz@bwh.harvard.edu](mailto:jlz@bwh.harvard.edu), or Galit Alter, [galter@mgh.harvard.edu](mailto:galter@mgh.harvard.edu).

The authors declare a conflict of interest. G.A. is a founder of SeromYx Systems.

**Received** 31 May 2022

**Accepted** 2 June 2022

**Published** 28 June 2022

pathogenesis (4) and can lead to additional selection and the outgrowth of viral variants (5). Thus, the development of therapeutics able to rapidly control and contain SARS-CoV-2 viral replication is key not only for the management of COVID-19 disease but also in preventing postinfection complications and the evolution of novel viral variants. The recent development of novel therapeutics able to reduce the risk of severe COVID-19 has effectively revolutionized our ability to fight against SARS-CoV-2; however, new small molecules still only provide partial effectiveness in those with most severe disease (6). Instead, both convalescent plasma and monoclonal therapeutics were deployed throughout the pandemic with the hope that these virus-specific therapeutics could effectively reverse the trajectory of disease. While convalescent plasma resulted in mixed results, monoclonal therapeutics displayed therapeutic benefit in early infection but poor benefit in late and severe COVID-19 (7, 8). However, monoclonal therapeutics were largely optimized for neutralizing antibody potency but did not fully explore the full functional potential of these unique therapeutics. However, whether additional antibody functions, beyond neutralization, are linked to enhanced clearance and control of the virus, particularly in the plasma, remains unclear.

There have been conflicting data on the role of the humoral immune response in resolution of COVID-19, with some studies reporting no significant association between viral load and anti-SARS-CoV-2 antibody responses, some studies pointing to higher antibody levels present in severe disease, and still other studies showing that monoclonal antibody therapy and host antibody development can reduce and control viral dynamics (9–11). However, many of these studies analyzed the effect of antibody development on upper respiratory tract viral dynamics, but respiratory tract viral loads do not always reflect levels of plasma RNAemia (3), the latter linked more closely to disease outcomes (1, 3). In addition, the longitudinal kinetics of antibody development, rather than a snapshot of antibody levels at a certain disease point, may be key to defining mechanisms of differential control of viral dissemination, as has been observed for predicting disease outcome (12). Moreover, studies have focused largely on binding and neutralizing activity, rather than the broader role of antibodies on leveraging the immune system to clear the virus and infected cells. Thus, it remains unclear whether the evolution of specific antibody functions or qualities may be key to antiviral control outside the respiratory tract. The insights gained from addressing this question could shed light upon the development of next-generation monoclonal therapeutics with expanded therapeutic capacity to prevent disease progression later in the course of infection. To this end, we sought to holistically profile the evolution of the SARS-CoV-2 humoral response with respect to the dynamics of RNAemia in a cohort of COVID-19 patients presenting just days after symptom onset.

## RESULTS

**Lower IgG3 and lower Fc $\gamma$ R binding levels track with higher RNAemia at the time of emergency department (ED) presentation.** While the kinetics of the evolution of the SARS-CoV-2-specific humoral immune response (12) and plasma RNAemia (1, 3) have both been associated with disease severity, it remains unclear whether SARS-CoV-2 antibodies track directly with differential systemic viral control. Using a cohort of acutely ill COVID-19 individuals, the relationship and kinetics of the humoral immune response were investigated. A total of 300 participants presenting to the emergency department (ED) with respiratory distress were included in this study, with 53 participants harboring RNAemia above the quantification range ( $2 \log_{10}$  copies/mL) and 53 with detectable RNAemia below the level of quantification ( $1.6 \log_{10}$  copies/mL) (1, 13). Approximately 40% of participants were at least 65 years old, 48% were female, 12% obese, 36% diabetic, and 48% hypertensive. In addition, 13% of participants had kidney disease, 21% had lung disease, 15% had heart disease, and 8% were immunocompromised. The median duration of symptoms before presentation was 7 days.

System serology was utilized to profile the evolution of the SARS-CoV-2-specific humoral immune response, capturing the evolution of distinct antibody isotypes and subclasses, IgG Fc $\gamma$ -receptor binding profiles, neutralization levels, and Fc-effector functions (monocyte phagocytosis, neutrophil phagocytosis, and complement deposition).

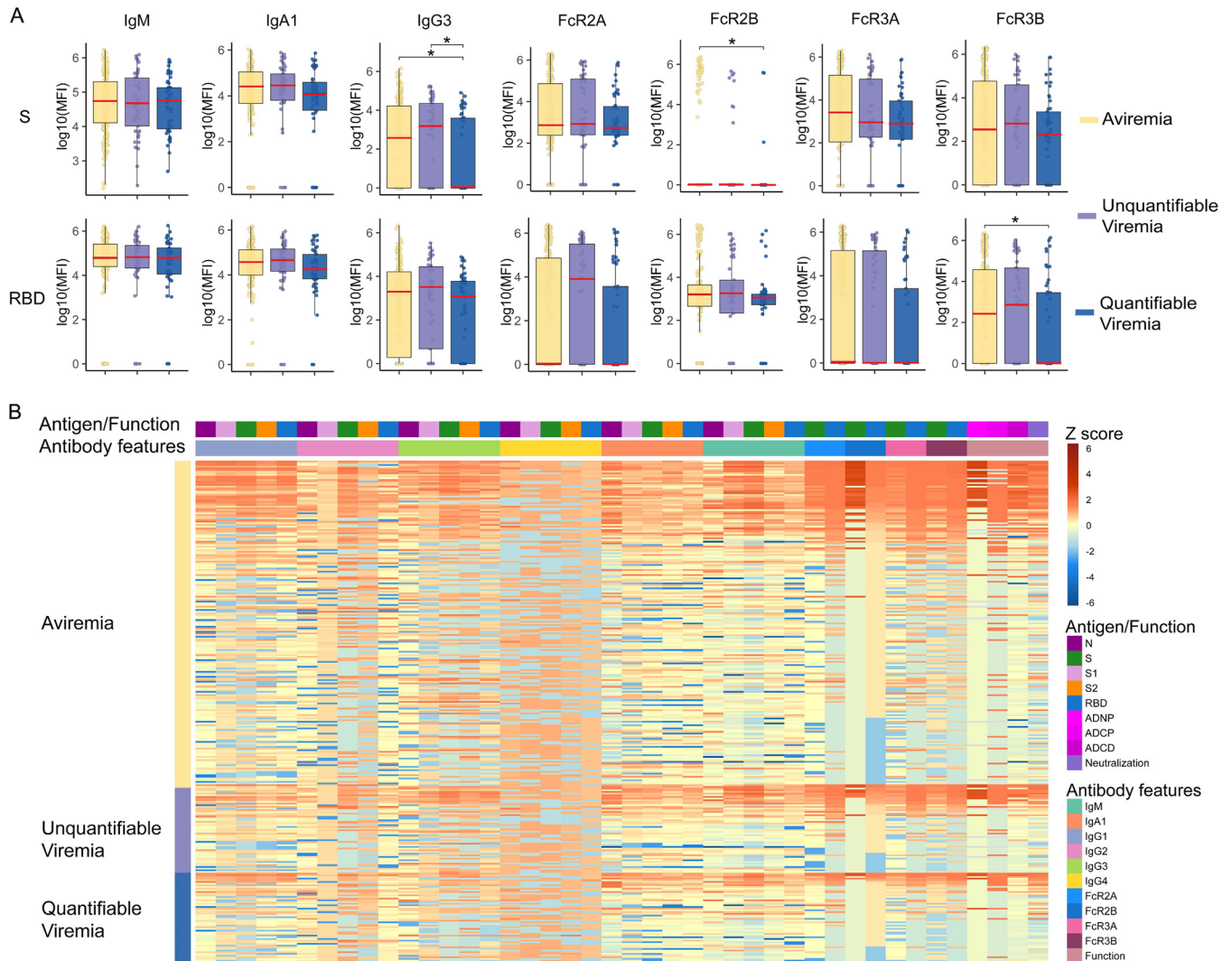


**FIG 1** Baseline antibody levels by levels of viremia. (A) Baseline S- and RBD-specific antibody features among different viremia groups ( $n = 300$ ). Three viremia groups' levels were compared using Mann-Whitney U tests with Benjamini-Hochberg correction (\*,  $P < 0.05$ ). Tukey boxplots were used to demonstrate the antibody levels and functions, with boxes indicating medians (red line) and interquartile ranges. Upper whiskers indicate the 75th percentile value plus  $1.5 \cdot$  interquartile range, and lower whiskers indicate the 25th percentile value minus  $1.5 \cdot$  interquartile range. (B) Heatmap summarizing baseline antibody features among three viremic groups.

For baseline analysis, all 300 participants were included. As shown in Fig. 1A, all the participants already had a detectable spike (S)-IgM antibody response. Elevated plasma RNAemia at the time of ED presentation was associated with lower S-specific IgG3 levels. IgG Fc-receptor spike receptor binding domain (RBD)-specific Fc $\gamma$ R3B and S-specific Fc $\gamma$ R2B binding were elevated in aviremic individuals compared to subjects with quantifiable RNAemia (Fig. 1A). Conversely, there were no significant differences in baseline antibody-dependent neutrophil phagocytosis (ADNP), antibody-dependent cellular phagocytosis (ADCP), and antibody-dependent complement deposition (ADCD) among different RNAemia groups (Fig. 1B; see Fig. S1 in the supplemental material).

**Persistence of plasma RNAemia is associated with increased COVID-19 mortality.** The essential role of antibodies in the elimination of viruses has been shown for pulmonary infections such as influenza (14), respiratory syncytial virus (15), and systemic pathogens including Ebola virus (16) and, most recently, malaria (17). To first determine whether viral clearance was associated with COVID-19 severity, we analyzed viral clearance dynamics in 86 viremic participants who were hospitalized and had more than one follow-up time point, permitting longitudinal analysis. While RNAemia trended down over time, a subset of participants did not fully clear their RNAemia

within 7 days of hospitalization (Fig. 2A). These individuals were grouped in the “viral persistence” category in contrast to individuals that cleared the virus at the second time point, also referred to as the “viral clearance” category.

The viral persistence and viral clearance groups had comparable duration of symptoms prior to ED presentation (seven versus 8 days,  $P = 0.30$ ), and the majority of participants presented to the ED within 15 days of symptom onset (Fig. S2A). Similar to our previous analyses in hospitalized patients (1, 3), baseline quantifiable plasma RNAemia at the time of ED presentation was associated with an increased mortality risk. Importantly, the presence of persistent RNAemia was independently associated with risk of death. Individuals with both quantifiable RNAemia at baseline and viral persistence had the greatest risk of death (44%, Fig. 2B), while those with unquantifiable baseline RNAemia and no evidence of viral persistence had the lowest risk of death (3%). The trajectory of RNAemia was further stratified by disease severity, and in both the viral clearance and persistence groups, those who survived COVID-19 demonstrated lower levels of RNAemia (Fig. 2C, Fig. S2B to D). Viral persistence was associated with an odds ratio (OR) of 5.8 (95% confidence interval [CI], 1.7 to 19.7;  $P = 0.005$ ) with mortality (Fig. 2D). After stratifying for baseline RNAemia and other baseline characteristics, viral persistence was consistently associated with increased mortality across different subgroups (Fig. 2D). Baseline kidney disease and hypertension were significantly associated with the persistence of RNAemia (Fig. S2E). Using RNA levels from day 7 as a surrogate for viral clearance, we also noted a significant association between death and day 7 RNA levels (Fig. S2F).

**Clearance of RNAemia tracks with SARS-CoV-2-specific antibody evolution.** We next evaluated the dynamics of RNAemia and antibody evolution across the same participants based on whether they experienced viral persistence or clearance. Early antibody responses, specifically IgM responses against S/S1/S2, were significantly different across the groups, at both day 0 and day 3 (Fig. 3A). SARS-CoV-2-specific IgG 1/2/3 against S and RBD were most different between the groups at day 3. However, by day 7, the clearance and persistence groups had comparable antibody levels (Fig. 3A). In parallel to IgG1/2/3 levels, SARS-CoV-2-specific Fc $\gamma$ R binding antibody levels also developed differentially across individuals who experienced viral persistence compared to those who cleared RNAemia. N-, S-, and S1/S2/RBD-specific responses all exhibited higher Fc $\gamma$ R2A/3A/3B binding levels at day 3 following admission in subjects that cleared infection compared to the subjects who experienced persistent RNAemia (Fig. 3B). Importantly, significantly higher levels of Fc $\gamma$ R3A and 3B binding related to RBD- and S2-specific antibodies were present in participants who cleared RNAemia as early as day 0 of the study.

Similar to antibody levels and Fc $\gamma$ R binding activity, the evolution of antibody function tracked with clearance of RNAemia. Antibody-dependent complement deposition (ADCD) and antibody-dependent cellular phagocytosis (ADCP) were higher at day 0 and day 3 in participants that cleared RNAemia compared to subjects with persistent RNAemia (Fig. 3C). Antibody-dependent neutrophil phagocytosis (ADNP) and neutralization levels (based on pseudovirus neutralization assay) showed a similar profile across the two groups at day 0 and day 7 but were significantly higher at day 3 in the clearance group (Fig. 3C). Overall, antibody functional profiles were compromised in individuals who exhibited prolonged RNAemia (Fig. 3D). In addition, the clearance group exhibited a more coordinated baseline antibody response at day 0, highlighted by higher levels of correlation across neutralization, ADCP, ADCD, and ADNP activity with several antibody features (IgG1 and IgA1 against all N/S/S1/S2/RBD, IgM against S/S1/S2/RBD, and Fc $\gamma$ R binding; Fig. 3E and Fig. S3). Conversely, the persistence group exhibited a less coordinated functional humoral immune response, highlighting differences not only in univariate humoral immune trajectory differences across the groups, but also in the coordination and deployment of multiple antibody functions that may contribute collaboratively to control viral replication, dissemination, and drive viral clearance. While age, sex, hypertension, and other characteristics showed no impact

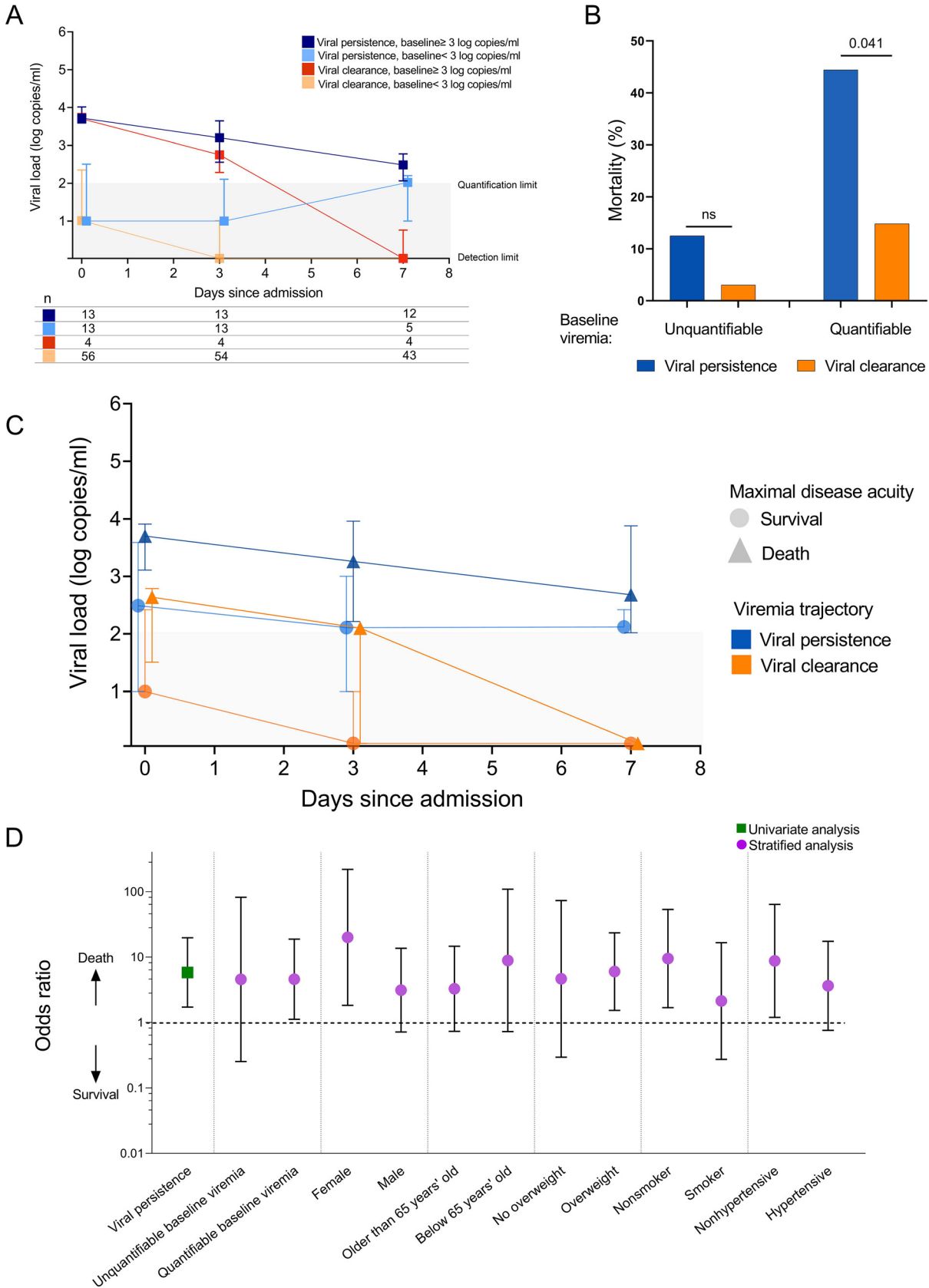


**FIG 2** Longitudinal trajectory of SARS-CoV-2 viremia. (A) Viremia trajectory stratified by baseline viremia level and viremia clearance ( $n = 86$ ). Medians and interquartile ranges are shown. (B) Viremia persistence is associated with mortality. Fisher's exact test was used to (Continued on next page)

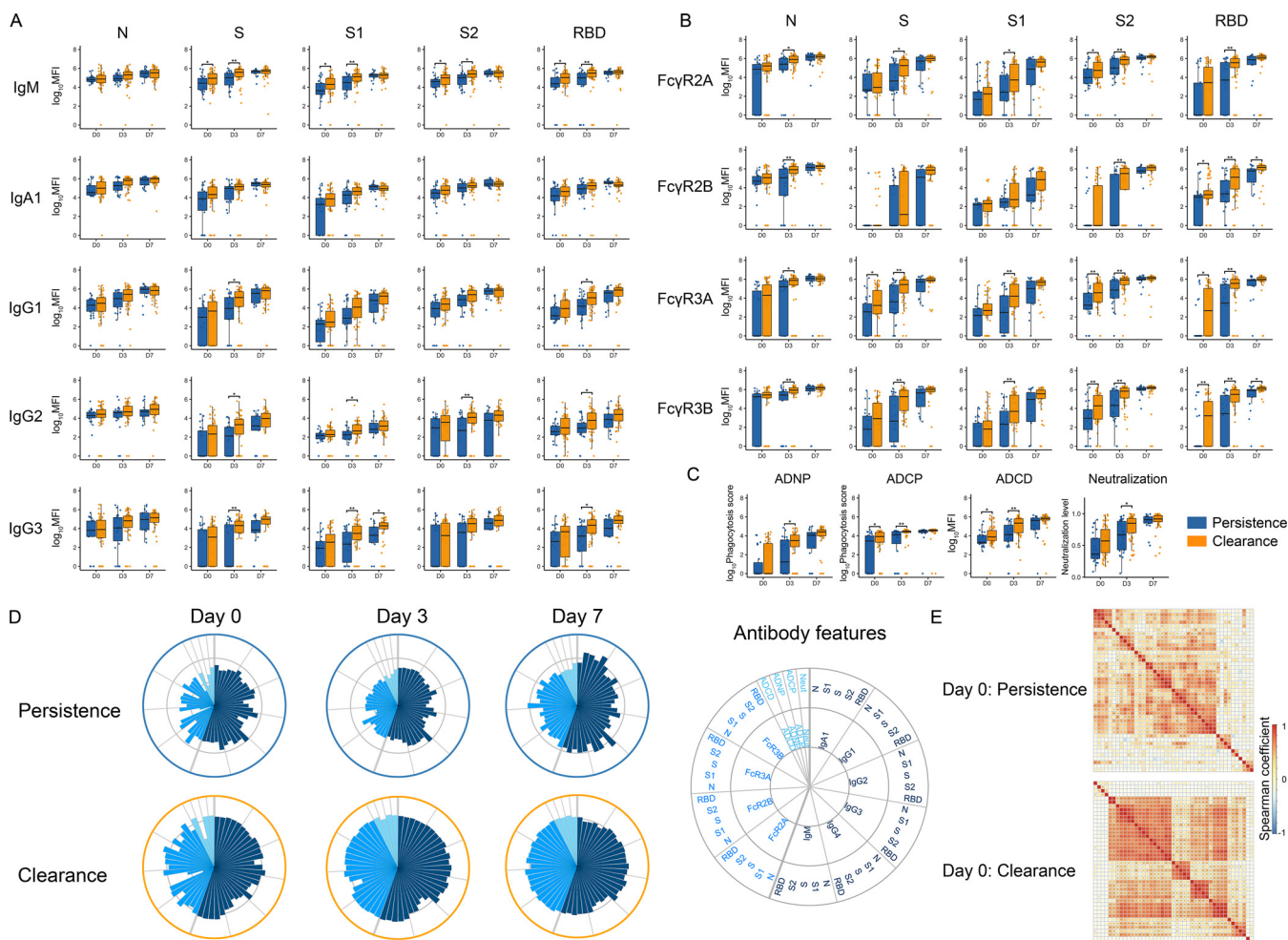


**FIG 3** Longitudinal antibody trajectories across individuals that cleared or experienced persistent viremia. Plasma samples ( $n = 234$ ) from 86 hospitalized SARS-CoV-2 infected individuals were profiled. (A to C) Distributions of (A) immunoglobulin titers, (B) Fc-receptor binding levels, and (C) antibody functions over admission days 0, 3, and 7 of hospitalization across viremia clearance (orange) and persistence (blue) groups. The whisker plots show the distribution, the solid black line represents the median, and the box boundary (upper and lower) represents the first and third quartiles. The dots show the scaled values of each sample. A two-sample Wilcoxon rank test was used to evaluate the differences between two groups for all the intervals and features. The  $P$  values were corrected from multiple hypothesis testing using the Benjamini-Hochberg procedure per each feature. Significance corresponds to adjusted  $P$  values (\*,  $P < 0.05$ ; \*\*,  $P < 0.01$ ). (D) The polar plots depict the mean percentile of each antibody feature at days 0, 3, and 7 across the persistence (top) and the clearance (bottom) groups. The major slices represent titer, Fc-receptors, and functions. The size of the wedge depicts the mean percentile, ranging from 0 to 0.75. (E) The Spearman correlation coefficient heatmap at day 0 across different participants who cleared viremia or experienced persistent viremia. Detailed information is shown in Fig. S3.

on the kinetics or quality of humoral evolution, kidney disease and immunosuppression were modestly associated with humoral evolution (Fig. S4), pointing to immunomodulatory states that may perturb humoral evolution and thus compromise viral clearance. Furthermore, utilizing the nested mixed linear models, we evaluated the association between each antibody level among 50 measurements and persistence/clearance group information by explicitly controlling the effects of these comorbidities, including lung disease, kidney disease, diabetes, hypertension, and demographic information, including age and body mass index (BMI) (see Materials and Methods). We still observed that IgG2/3 against S1 and RBD, and IgG3 against S were enriched in the clearance group. Additionally, we observed that N-, S- and S1/RBD-specific responses

**FIG 2** Legend (Continued)

evaluate the statistical differences between the persistence and clearance groups. (C) Viremia trajectory stratified by COVID-19 disease outcome. Medians and interquartile ranges are shown. (D) Odds ratio of death in those with viral persistence in a univariate analysis (green square) and in logistic regression (purple circles) stratified by baseline viral load, demographics, and other potential mediators of increased mortality. Odds ratios with 95% confidence intervals were demonstrated.

all exhibited higher Fc $\gamma$ R binding levels in the subjects with cleared infection than in those who experienced persistence. These results were consistent with univariate analysis without cofounder correction to suggest that clearance of RNAemia tracks with SARS-CoV-2-specific antibody evolution.

**S2-, S-, and RBD-specific Fc-profiles distinguish clearance and persistence at day 3.** Given the multitude of humoral immune differences across subjects that cleared or exhibited persistence of RNAemia, we next aimed to define a minimal set of SARS-CoV-2 humoral signatures that account immunologically for systemic viral control and clearance. Least absolute shrinkage and selection operator (LASSO) feature selection (18) was performed first to collapse the multitude of correlated humoral features into a minimal set that maximally could account for variation in clearance of RNAemia. Separation between individuals that cleared the virus or exhibited persistence was then visualized using a partial least-squares discriminant analysis (PLSDA). Focusing on day 3, where the most significant univariate differences were observed, 74% of the variability across the groups could be explained by the first two latent variables (LVs) using as few as 4 selected features of the 50 total features that were captured for each plasma sample (Fig. 4A). The 4 features were S2-specific IgA1, S2-specific IgG2, S2-specific IgG3, and RBD-specific Fc $\gamma$ R3A binding levels (Fig. 4B). Furthermore, given that the features selected during down-selection may represent additional cocorrelated humoral features that may provide additional mechanistic insights into the polyclonal mechanisms involved in elimination of RNAemia, we next built a cocorrelate network between selected features by LASSO and nonselected features. As shown in Fig. 4C, a single large cocorrelate network appeared, including the 4 model-selected features (large nodes), linked to additional highly correlated features (smaller nodes) pointing to a broader array of S1/S2/S-specific Fc $\gamma$ R3A binding, RBD-specific Fc $\gamma$ R2A/2B binding, and RBD-specific IgG1/IgG3, which likely collectively form a polyclonal response required for effective viral capture and clearance. In addition, the model performance was evaluated using 5-fold cross validation to test the significance of the model. The original model outperformed permuted controls (Fig. 4D). Additionally, we used the RNAemia value on day 7 as a continuous variable and further evaluated whether the similar humoral signatures were identified to associate with the continuous RNAemia. We performed a partial least-squares regression (PLS-R) analysis (Fig. S5) and observed that S2-specific IgA1 and S-specific IgG3 were also selected in this regression model. Additionally, through the correlation analysis, we observed that RBD-specific Fc $\gamma$ R3A binding, selected in the classification model, was also highly correlated with S2-specific Fc $\gamma$ R2A binding, which was selected in our regression model.

**Antibody evolutionary kinetics distinguish clearance and persistence.** Beyond differences in the humoral immune response at discrete time points, we next aimed to explore kinetic differences in the evolution of the humoral immune response to further mechanistically define the importance of distinct humoral features in clearance of RNAemia over time. Thus, SARS-CoV-2-specific responses were modeled based on time from symptom onset. Locally estimated scatterplot smoothing (LOESS) curves demonstrated significant differences in the evolutionary kinetics of all humoral features across the groups, marked by similar early responses, which plateaued lower in the persistence group, rapidly decaying to lower levels than those observed in the clearance group (Fig. S6). To quantify these differences, quadrimetric modeling was applied to these data (Fig. 5A and B, Fig. S7) to probe the specific differences in each humoral immune parameter based on initial levels at either the time of symptom onset (parameter a), in the initial rise or conversion speed (parameter b), in the time to half-seroconversion (parameter c), or in the ultimate final plateau level (parameter d) (Fig. 5A). The Akaike information criterion (AIC) was used to determine the best model for each antibody feature. Interestingly, initial levels were generally comparable across the groups, although higher levels of S-IgG2 were observed in the persistence group in contrast to the higher N-specific IgG3, S1-Fc $\gamma$ R2b, S1-Fc $\gamma$ R3A, and RBD-specific Fc $\gamma$ R3B observed in the clearance group (Fig. 5C). Surprisingly, a faster initial rise and time to half-seroconversion was observed for most features in those who experienced viral persistence,

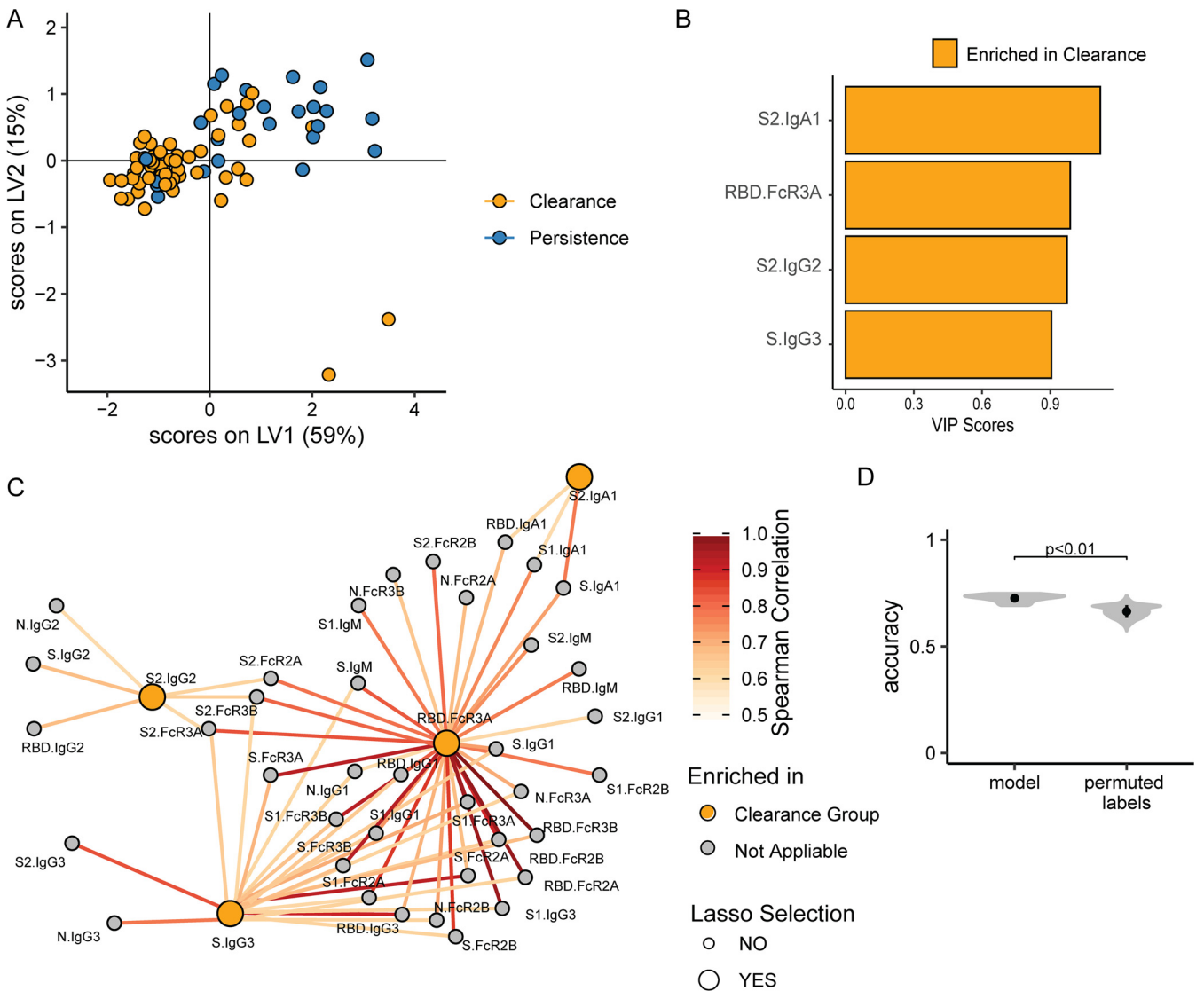


**FIG 4** Multivariate analysis of antibody profiles across individuals that cleared or experienced persistent viremia. (A) Focusing on day 3, the PLSDA score plot demonstrates the degree of discrimination across individuals that cleared viremia or that experienced persistent viremia after LASSO feature down-selection. Each dot represents an individual; blue, persistence; orange, clearance. (B) The bar plot shows variable importance in projection (VIP) scores of the LASSO selected features. The magnitude of the bars indicates the importance of the feature in driving separation in the model. The color of the bar represents the group in which the feature is enriched. (C) The correlation network demonstrates the cocorrelated features (small nodes) that are significantly correlated with the model-selected features (large nodes). Edge color corresponds to the correlation strength. Here, only the significant Spearman correlation coefficients larger than 0.6 after Benjamini-Hochberg multiple testing correction are shown. (D) The violin plots show the distributions of repeated classification accuracy tests using the actual data and shuffled labels, illustrating the performance and robustness of the model. Black circles indicate the median accuracies with one standard deviation.

with the exception of the initial features that were enriched in individuals with rapid RNAemia clearance (Fig. 5C). However, plateau magnitudes were largely elevated in individuals with rapid clearance of RNAemia, except for N-specific IgG4, a marker of a less functional humoral immune response in people with COVID-19. Among the antibody functions, ADCP, ADBP, and ADCD all plateaued at higher levels in the clearance group, while neutralization did not differ across the groups over time. These data collectively point to a highly specific early humoral immune response, marked by IgG3 and Fcγ-receptor binding characteristics that may be key for initial viral control, and the deficiencies in humoral immune responses linked to viral persistence (Fig. 5C).

To finally define the antibody evolutionary profiles that differed most across the groups, changes in AIC values for each antibody feature were listed to determine features that showed the greatest variation between individuals that cleared RNAemia or



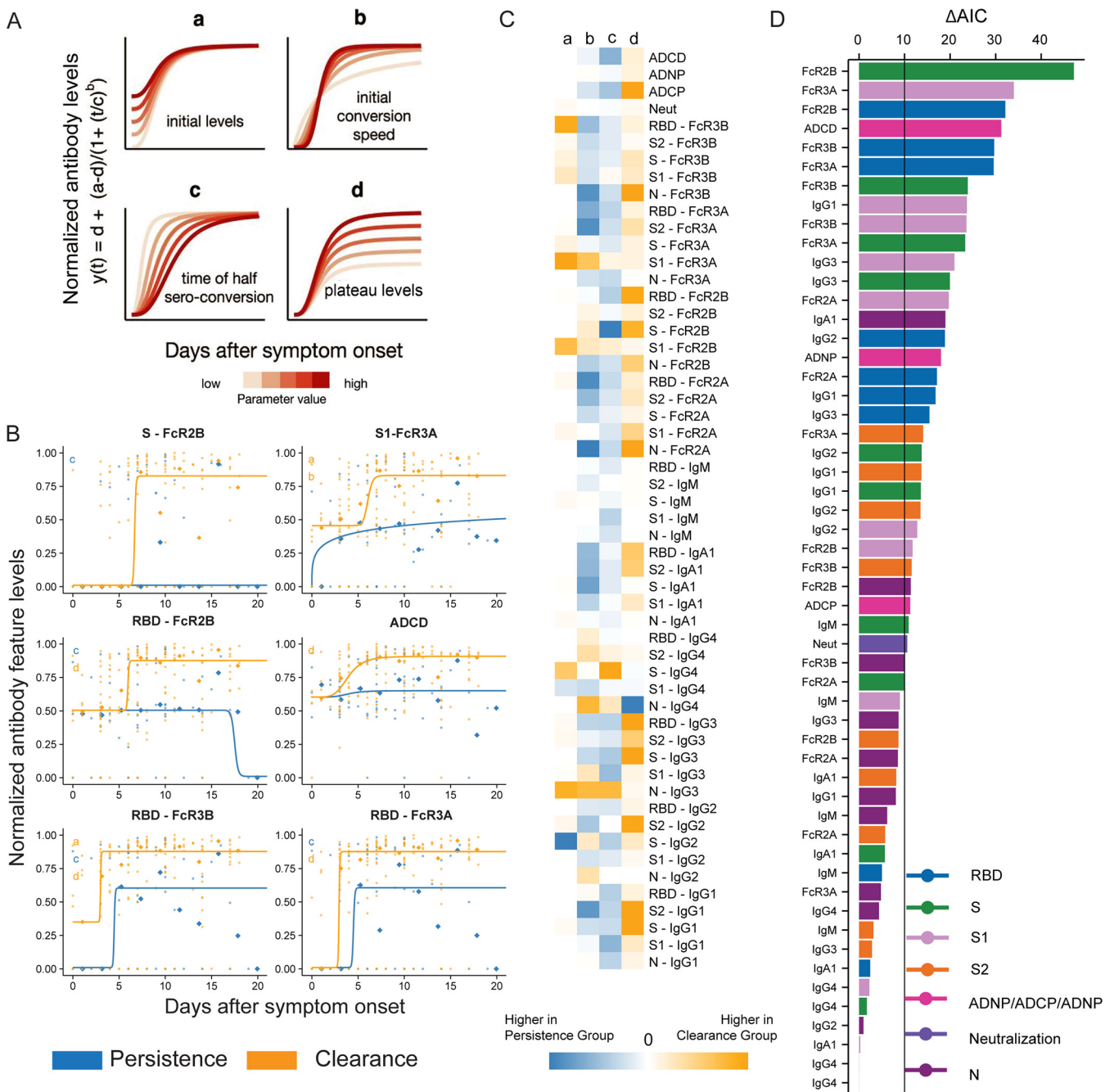


**FIG 5** Modeling kinetics of antibody-mediated control of viremia. (A) The cartoon highlights the breakdown of the four-parameter logistic growth curve (a, initial levels; b, initial seroconversion speed; c, seroconversion time; d, endpoint levels) used to model the mechanism of antibody-mediated control of viremia. The influence of each parameter on the shape of the curve is shown for various parameter values. (B) The top six antibody features with highest  $\Delta AIC$  values are shown as individual graphs depicting striking differences in kinetics across the two group-based days since symptom onset. Diamond-shaped dots indicate the binned median of measurements, and round dots indicate the measurement for each individual at certain time points. (C) The heatmap shows the AIC weight-averaged parameter differences between individuals that cleared viremia (yellow) or experienced persistent viremia (blue). The intensity of the color highlights the intensity of the enrichment of the feature in either group. Dots indicate individual patients, diamonds indicate the binned median, the curves indicate the optimal fitted models, and the colors indicate the groups. The parameters shown in the left corner are different for the displayed model and color-coded according to the group for which the parameter is higher. (D) The bar graph shows the  $\Delta AIC$  of the four-parameter models. The bar heights are ranked based on features that explain trajectory differences best-to-worst- across the persistence and clearance groups. The vertical line ( $\Delta AIC = 10$ ) indicates the commonly used threshold for rejecting models.

experienced the persistence of RNAemia (Fig. 5D). Fc $\gamma$ R binding levels dominated the top 10 most differential humoral immune features, marked by highly divergent S-, RBD-, and S1-specific titers and AD/CD activity. Moreover, changes in longitudinal levels highlight temporal differences for each of the top 6 humoral features, pointing to a

potential critical initial expansion of RBD-specific Fc $\gamma$ R3B at the time of symptom onset in the viral clearance group, followed by rapid evolution of S- and RBD-specific Fc $\gamma$ R2B binding antibodies, which stands in contrast to the low and waning levels found in the viral persistence group (Fig. 5B, Fig. S7). To evaluate the robustness of the model fit, we fit the model using 85% of the sample data randomly in three independent replicates and summarized the resulting most discriminatory features (Fig. S8A and B). The top 30 shared features were ordered based on their  $\Delta$ AIC and the proportions were visualized using Venn diagrams (Fig. S8C). These data demonstrate the repeated emergence of shared discriminatory features across each analysis, further pointing to the importance of specific antibody Fc-binding and functional characteristics that may be key for therapeutic activity of SARS-CoV-2 antibodies in the setting of an evolving humoral immune response in COVID-19.

## DISCUSSION

In the wake of the completion and early termination of several large convalescent plasma and monoclonal therapeutic trials (8, 19–21), whether and how antibodies contribute to viral control and clearance in the setting of severe disease remains unclear. Monoclonal therapeutics have been shown to confer benefit prior to the evolution of the natural humoral immune response (11). However, naturally evolving antibody functions have been linked to survival and clearance across several studies (9, 12). Thus, in this study, we sought to define the specific antibody functional profiles that track with antiviral control and the resolution of COVID-19, focusing on the dynamics of SARS-CoV-2 RNAemia, known to be strongly associated with clinical outcomes. Here, we observed a strong linkage between RNAemia and particular SARS-CoV-2-specific antibody Fc-characteristics, pointing to the early importance of IgG3, S1/RBD Fc $\gamma$ -receptor binding activities, and evolution of broad Fc $\gamma$ R and opsonophagocytic functions in individuals that rapidly clear SARS-CoV-2 RNAemia. These data highlight the critical role of particular Fc-receptor functions as key functional determinants that may be essential for clearance of SARS-CoV-2 RNAemia, in the setting of a massively proliferating antiviral immune response, which may be key to resolution of severe disease.

We and others have previously reported in cross-sectional studies that detectable SARS-CoV-2 RNAemia and viral dissemination is associated with increased risk of severe COVID-19 and mortality (1, 3, 22, 23), which appears to be mediated by increased systemic inflammation, endothelial and tissue damage, and perturbation of the coagulation cascade (1, 24). While prolonged RNAemia has been described in immunosuppressed individuals (4, 25), its role in predicting disease severity in the general population has remained unclear. In this study, we further demonstrated that failure of prompt SARS-CoV-2 RNAemia clearance is an independent predictor of maximal COVID-19 severity and risk of mortality, even after adjusting for baseline levels of RNAemia and other potential confounders. These findings provide important context on the importance of identifying immune factors that lead to rapid clearance of plasma RNAemia. Our findings are consistent with cohort studies from other medical centers that suggest that longer duration of RNAemia and lower RBD-specific IgG responses are related to worse COVID-19 outcomes (23, 26, 27), extending these observations to the specific antibody characteristics that may underly antibody-mediated antiviral clearing activities.

Previous studies have pointed to early antibody functional evolution as a correlate of natural resolution of COVID-19 (9, 10, 12). However, whether specific humoral changes were linked to systemic control of RNAemia, and thus to control of viral dissemination and broader disease, was unclear. In our current study, we revealed that early development of certain antibody features (S-IgG3, S-Fc $\gamma$ R2B binding, and RBD-Fc $\gamma$ R3B binding) are associated with absence of RNAemia in the early course of disease. However, in people who had detectable viremia at the time of emergency department presentation, rapid and robust evolution of broad Fc-receptor binding profiles and functions are tightly linked to the kinetics of viremia clearance. These data are consistent with earlier reports suggesting that the timing and maintenance

of antibody functions, rather than cross-sectional antibody levels and neutralization titers, are more tightly associated with COVID-19 outcomes (12). Similarly, in a New Haven cohort, 50% of discharged COVID-19 participants mounted neutralizing antibodies in the first 7 to 9 days of symptom onset, compared to slower kinetics (~14 days) in those who ultimately passed away (9). Delayed humoral immune evolution may be explained by defective Bcl-6-expressing T follicular helper cell evolution in severe/fatal COVID-19 leading to delayed and defective humoral immune evolution (28). Thus, collectively, our data demonstrate that early and rapid antibody development, especially certain SARS-CoV-2 spike-specific IgG Fc $\gamma$ R binding properties, may contribute centrally to the prevention of viral dissemination and, more importantly, clearance of viral dissemination once RNAemia develops.

While convalescent therapy and monoclonal therapeutics have shown efficacy in individuals with low-level baseline SARS-CoV-2 antibody titers during early presentation (29), these therapeutics have shown more limited impact following the evolution of the humoral immune response (7, 8, 11, 21). This modest effect during progressive disease may relate to the necessity for antibody therapeutics to compete for immune complex occupancy with naturally evolving humoral immune responses, which may become progressively more difficult as the humoral immune response evolves. The data presented here, however, may provide an additional explanation for the modest performance of these antiviral therapies, related to the importance of antibodies to bind more effectively to Fc-receptors (30) and aggressively draw on innate immune function early in disease to reprogram the activity of evolving immune complexes. In a mouse model, Suryadevara and colleagues demonstrated that Fc $\gamma$ R binding is required for the therapeutic activity of 2 monoclonal therapeutics (COV2-2676 and COV2-2489) following SARS-CoV-2 infection (31). Similarly, Yamin and colleagues demonstrated that optimizing Fc $\gamma$ R binding via monoclonal antibody (MAb) engineering was associated with better protection against SARS-CoV-2 (32). These findings were further confirmed in a live-imaging mouse model demonstrating that Fc $\gamma$ R-effector cell interaction was crucial in preventing severe disease by dampening inflammatory responses (33). Along these lines, recent correlate analysis from the CONCOR-1 convalescent plasma study pointed to the enrichment of elevated antibody-dependent cellular cytotoxicity (ADCC) in survivors compared to deceased individuals (21). Furthermore, the competition of monoclonal antibodies with the more multifaceted host humoral immune responses could help explain the link between signals of treatment antagonism with worse outcomes in hospitalized patients who already have a developed humoral immune response (7, 8). Thus, emerging next-generation monoclonal antibodies have begun to explore the potential addition of Fc-enhanced monoclonal drugs, which may contribute functionally to the evolving humoral immune response, shifting and potentiating antiviral control and clearance in a way that has not been explored by current Fc-silent or simple IgG1 backbones to date.

Because the participants in this study presented to the ED with various durations of symptoms, which were subjectively reported, we aligned all the samples from different individuals based on day of symptom onset and performed quantitative kinetics modeling to ensure that our findings still hold true. This analysis provided critical assurances that differences in kinetics were not attributable to simple differences in time from infection. Peripheral blood mononuclear cells (PBMC) were also collected in this cohort, but SARS-CoV-2-specific T cell analyses have not been performed in this cohort. Additional large collections are under way to begin to probe the complementary role of antibody effector functions and T cells in control of RNAemia (34, 35). However, despite these limitations, the study presented here, linking SARS-CoV-2 RNAemia dynamics and virus-specific antibody evolution, points to critical humoral functions that may play a key role in preventing dissemination and contributing to control and clearance of the disease. These results provide insights for next-generation monoclonal therapeutic design, especially in the face of new variants, including Omicron (36, 37).

## MATERIALS AND METHODS

**Participants.** Participant enrollment was described in our prior studies (1, 13). Participants were enrolled in the emergency department (ED) from Massachusetts General Hospital, Boston, MA, from 24 March 2020 to 30 April 2020 during the first peak of the COVID-19 surge, with an institutional review board (IRB)-approved waiver of informed consent. Inclusion criteria for this cohort included COVID-19-related symptoms, adults, and nucleic acid test confirmation of SARS-CoV-2 infection. Clinical course was followed to 28 days postenrollment or until hospital discharge if that occurred after 28 days.

**Plasma SARS-CoV-2 RNAemia quantification.** Plasma SARS-CoV-2 viral load measurement was reported in our previous study (1, 13). Briefly, RNA was extracted from 300  $\mu$ L of RPMI 1640-diluted EDTA-preserved plasma sample (RPMI 1640:plasma 2:1 dilution) (1, 13) using a TRIzol-based method (Thermo Fisher Scientific, Waltham, MA). SARS-CoV-2 viral load was quantified using the U.S. CDC2019-nCoV\_N1 primers and probe set (3). Viral load reverse transcriptase PCR (RT-PCR) assays were performed in triplicate. The lower limit of SARS-CoV-2 N gene quantification was 100 copies/mL. Samples with a positive signal but viral load of <100 copies/mL were denoted detectable but unquantifiable and were given a value of 10 copies/mL (1 log copy/mL).

**RNAemia clearance.** The majority of participants only had blood samples from days 0, 3, and 7 of hospitalization available. Thus, it is difficult to categorize their RNAemia clearance based on a snapshot of day 7 viral load with limited duration of follow-up, given that participants with different baseline RNAemia levels may exhibit different viral load dynamics between day 0 and day 7 (Fig. 2A). We define RNAemia clearance based on RNAemia level at day 0:

- For participants with day 0 viral load of  $\geq 3$  log copies/ml: day 7 viral load at least unquantifiable (<2 log copies/mL) or day 3 viral load at least unquantifiable (<2 log copies/ml if day 7 viral load not available).
- For participants with day 0 viral load of <3 log copies/mL: day 7 viral load undetectable or day 3 viral load at least unquantifiable (<2 log copies/mL if day 7 viral load not available).

Those who did not satisfy these criteria were categorized in the RNAemia persistence group.

In addition, there were four participants with baseline day 0 viral load unquantifiably detectable but that only had day 3 follow-up sample available. All four participants had day 3 viral load unquantifiably detectable. These four participants were grouped in the persistence group.

**Luminex-based antibody levels and Fc $\gamma$ R binding assays.** Antigen-specific antibody subclasses and Fc $\gamma$ R binding levels were measured using a 384-well-based customized multiplexed Luminex assay as previously described (14). In this study, the following antigen-specific antibody levels were measured using this high-throughput platform SARS-CoV-2 nucleocapsid (N) protein (Aalto Bio Reagents), SARS-CoV-2 spike protein (S) (kindly provided by Eric Fischer, Dana Farber), S1 (Sino Biological; 40591-V08B1), S2 (Sino Biological; 40590-V08B), and SARS-CoV-2 RBD (kindly provided by Aaron Schmidt, Ragon Institute). Briefly, antigens were covalently bound to fluorescent carboxyl-modified microspheres (Luminex) by *N*-hydroxysuccinimide (NHS)-ester linkages using 1-Ethyl-3-(3-dimethylaminopropyl) carbodiimide (EDC) and sulfo-NHS (Thermo Scientific). Antigen-coupled beads were then washed and blocked before adding plasma samples at an appropriate sample dilution (1:500 for IgG1, 1:1,000 for all Fc $\gamma$ -receptors, and 1:100 for all other isotype/subclass readouts). The sample then underwent an overnight incubation at 4°C with shaking at 700 rpm, followed by washing with an automated plate washer (Tecan) with 0.1% bovine serum albumin (BSA) and 0.02% Tween 20. Antigen-specific antibody titers were detected using a phycoerythrin (PE)-coupled detection antibody for each subclass and isotype (IgG1, IgG2, IgG3, IgA1, and IgM; Southern Biotech), and Fc-receptors were fluorescently labeled with PE before addition to immune complexes (Fc $\gamma$ R-2A, -2B, -3A, and -3B; Duke Protein Production facility). Plasma samples were acquired via flow cytometry, using an iQue (IntelliCyt) platform and S-LAB robot (PAA). Analysis was done using ForeCyt software by gating on fluorescent bead regions, and PE median fluorescent intensity (MFI) was reported as the readout for antigen-specific antibody titers and Fc $\gamma$ R binding levels.

**Effector function assays.** Bead-based assays were used to quantify antibody-dependent cellular phagocytosis (ADCP), antibody-dependent neutrophil phagocytosis (ADNP), and antibody-dependent complement deposition (ADCD) as previously described (12, 38). Briefly, yellow (ADNP and ADCP) as well as red (ADCD) fluorescent neutravidin beads (Thermo Fisher) were coupled to biotinylated SARS-CoV-2 RBD, N, and S antigens and incubated with diluted plasma (ADCP and ADNP 1:100, ADCD 1:10) to allow immune complex formation for 2 h at 37°C.

For ADCP, THP-1 cells (ATCC) were added to the immune complexes at  $1.25 \times 10^5$  cells/mL and incubated for 16 h at 37°C. Events were gated on singlets and bead-positive cells.

For ADNP, HL-60 cells were differentiated into CD11-expressing neutrophils and then to immune complexed yellow beads and incubated for 16 h at 37°C. Afterward, neutrophils were stained with an anti-CD11 BV605 detection antibody (BioLegend) and fixed with 4% paraformaldehyde (Alfa Aesar). Events were gated on CD11<sup>+</sup> bead<sup>+</sup> neutrophils.

For ADCD, lyophilized guinea pig complement (Cedarlane) was reconstituted and diluted in gelatin veronal buffer with calcium and magnesium (GBV++) (Boston BioProducts). Subsequently, C3 was detected with an anti-C3 fluorescein-conjugated goat IgG fraction detection antibody (MP Bio). ADCD was reported as the median of C3 deposition.

All assays were acquired via flow cytometry with an iQue (IntelliCyt) platform and an S-LAB robot (PAA). Phagocytosis scores were calculated for ADCP and ADNP as (percentage of bead-positive cells)  $\times$  (MFI of bead-positive cells) divided by 10,000.

**Neutralization.** The pseudovirus-based neutralization assay was reported in our prior study (13). Briefly, lentivirus vector was constructed using PCR amplification (Q5 high-fidelity 2 $\times$  master mix; New England

Biolabs) from pUC57-nCoV-S (gift of Jonathan Abraham) and further fused to HIV-1 gp41 to obtain pCMV-SARS2ΔC-gp41. 293T cells were transfected with 1 μg psPAX, 1.6 μg pTRIP-SFFV-EGFP-NLS (Addgene), and 0.4 μg pCMV-SARS2ΔC-gp41 using TransIT-293 transfection reagent (Mirus Bio). After overnight incubation, the medium was changed. SARS-CoV-2 S pseudotyped lentiviral (Wuhan-Hu-1 strain) particles were collected 30 to 34 h post-medium exchange and filtered using a 0.45-μm syringe filter. One day before the neutralization experiment, 293T ACE2/TMPRSS2 cells were seeded at  $5 \times 10^3$  cells in 100 μL per well in 96-well plates. On the day of lentiviral harvest, 100 μL SARS-CoV-2 S pseudotyped lentivirus was incubated with 50 μL of plasma diluted in medium to a final concentration of 1:100. Medium was then removed from the 293T ACE2/TMPRSS2 cells and replaced with 150 μL of the mix of plasma and pseudotyped lentivirus. Wells in the outermost rows of the 96-well plate were excluded from the assay. After overnight incubation, medium was changed to 100 μL of fresh medium. Cells were harvested 40 to 44 h postinfection with TrypLE (Thermo Fisher), washed in medium, and fixed in fluorescence-activated cell sorter (FACS) buffer containing 1% paraformaldehyde (PFA; Electron Microscopy Sciences). The percentage of green fluorescent protein (GFP) was quantified on a CytoFLEX LX instrument (Beckman Coulter), and data were analyzed with FlowJo. The events recorded by the flow cytometer do not suggest cell loss due to detachment. Neutralization rate was defined as  $1 - (\text{GFP\% pseudovirus} + \text{plasma/GFP\% pseudovirus alone})$ .

**Statistics.** Continuous variables were summarized using medians and interquartile ranges (IQRs). For clinical variables, we used the Mann-Whitney test to compare continuous variables from two different categorical groups and Dunn's test with the Benjamini-Hochberg *post hoc* test for three or more groups. Categorical variables were evaluated using the  $\chi^2$  test or Fisher's exact test. We used Spearman's rank correlation coefficient to evaluate correlation between different continuous variables. To evaluate the association of SARS-CoV-2 RNAemia clearance and clinical outcomes, we used logistic regression analyses to calculate odds ratios (OR) and 95% confidence intervals (CI). Clinical data analyses and logistic regression were performed on Stata (version 13.1), and figures were generated by Stata and GraphPad Prism (version 9.1). R (version 4.0.0) and Python (version 3.6.8) were used to analyze antibody data as described below.

**Temporal analysis.** The full methods were described in our recent study (12). Briefly, all antibody features were subtracted by phosphate-buffered saline (PBS) control values and then  $\log_{10}$  transformed. After that, the values were normalized to a (0, 1) scale such that the minimal value equals 0 and the maximal value equals 1. First, a nonparametric regression model was used to obtain a smoothed line using the R function *loess* (span = 0.7). Of note, the late rise and fall of some curves is attributable to a limited number of late time points and not due to a true elevation in antibody levels.

Four-parameter logistic growth curve regression was described in our recent study (12).

$$y(t) = d + \frac{a - d}{\left(1 + \left(\frac{t}{c}\right)^b\right)}$$

In this equation, the four parameters denote the following features: *a*, the initial antibody levels upon symptom onset; *b*, the initial seroconversion speed; *c*, the time of 50% seroconversion; and *d*, the plateau end levels. In order to compare antibody dynamics from clearance and persistence groups, models were built for these two groups simultaneously, allowing for combinations of parameters to differ between the groups, leading to  $2^4 = 16$  models. For each feature, each of the 16 models was fitted to the data using maximum likelihood estimation (Laplacian likelihood function to handle outliers), treating each measurement as an independent data point and assuming that differences in measurements arose due to measurement noise. We used the Akaike Information Criterion (AIC) to decide which particular differences were most distinct across two groups (39). The model with the lowest AIC value was then chosen to be the best model.

**Association analysis between measured antibody levels and persistence/clearance by controlling potential cofounders.** Utilizing a nested mixed linear model (null and full model) with/without comorbidities and physical information, we assessed the significance of the association between antibody-related measurements and defined persistence/clearance group information. Using samples caught within 21 days since symptom onset, we fit 2 linear mixed models and estimated the improvement of model performance using a likelihood ratio test for each measurement. Then, we evaluated the significance of the association as the improvement of model performance ( $P \leq 0.05$ ) and the coefficient of the persistence/clearance group information. The details of the nested linear mixed models are shown as follows:

Null model:

$$\text{antibody measurement}_{ij} \sim 1 + \text{Age}_i + \text{BMI}_i + \text{Heart}_i + \text{Lung}_i + \text{Kidney}_i + \text{Diabetes}_i + \text{HTN}_i \\ + \text{ImmunoRepression}_i + \text{SymOnset}_{ij} + (1|\text{Pat.ID}_i)$$

Full model:

$$\text{antibody measurement}_{ij} \sim 1 + \text{Persistence?}_i + \text{Age}_i + \text{BMI}_i + \text{Heart}_i + \text{Lung}_i + \text{Kidney}_i \\ + \text{Diabetes}_i + \text{HTN}_i + \text{ImmunoRepression}_i + \text{SymOnset}_{ij} + (1|\text{Pat.ID}_i)$$

Likelihood ratio test:

$$LRT = -2 * \ln \left( \frac{MLE \text{ in full model}}{MLT \text{ in null model}} \right) \sim \lambda^2$$

Here, demographic information including age and body mass index (BMI) and the binary status of historical diseases including heart disease, lung disease, kidney disease, diabetes, hypertension (HTN), and immunosuppression status were included into the models as fixed potential confounders/effects. Additionally, the day of symptom onset (SymOnset) was incorporated into the model, and the different initial values (intercept) of measurement among different patients were included as a random effect.

The R package lme4 was used to fit two nested models to each measurement. The *P* value from the likelihood ratio test and the *t* value (normalized coefficient) of the persistence/clearance group information in the full model were visualized as a volcano plot using the ggplot function in the R package ggplot2.

**Partial least-squares discriminant analysis (PLSDA)/partial least-squares regression analysis (PLS-R).** First, we applied the least absolute shrinkage and selection operator (LASSO) feature selection algorithm to extract significant features. We ran LASSO 10 times on the whole data set and identified the set of features in more than 60% of the repetitions, which were implemented in the function select\_lasso in the systemseRology R package (version 1.0). The PLSDA model was built using the extracted features. Model performance was evaluated by 5-fold cross-validation, and negative-control models were constructed from permuted data with 100 iterations. For PLS-DA, we used the opls function in the roppls R package (version 1.22.0) for classification and functions in the systemseRology R package for the purpose of visualization. Model training details were reported in our recent system serology study on SARS-CoV-2 (40). A partial least-squares discriminant analysis (PLS) classifier was then trained using the fold-specific selected features to predict the test set. Multiple iterations of fold-specific feature selections were performed to obtain a single model. This process was repeated over 20 replicates, and convergent correlates were observed. The performance and robustness of the model were contrasted with those of negative-control models from permuted data with 100 iterations of 5-fold cross-validation to generate classification accuracy. In detail, the permuted control was generated by shuffling labels randomly for each time. Robustness was defined as the effect size of distributions and the exact *P* values of the tail probabilities of the actual distribution with the control distribution. For the regression analysis, the same procedure was applied to the data set, and PLS-R in the roppls R package function was used to evaluate the association between selected features and the continuous response (RNAemia values).

**Correlation networks.** We constructed correlation networks to visualize the additional humoral immune features that were significantly linked to the selected minimal antibody features. In brief, antibody features that were significantly correlated with a Holms-Bonferroni correction to the final selected PLS model selected features were defined as cocorrelates. Significant Spearman correlations above a threshold of  $|r| \geq 0.6$  were visualized within the networks. For implementation, Spearman correlation coefficients were calculated using the rcorr function in the Hmisc package (version 4.4.2), and the *P* values were corrected by Benjamini-Hochberg correction in the stats package (version 4.0.3). Finally, the networks were visualized using the ggraph and igraph packages with proper manual adjustment.

## SUPPLEMENTAL MATERIAL

Supplemental material is available online only.

**FIG S1**, TIF file, 1.5 MB.

**FIG S2**, TIF file, 0.6 MB.

**FIG S3**, TIF file, 2.8 MB.

**FIG S4**, TIF file, 1.5 MB.

**FIG S5**, TIF file, 1.2 MB.

**FIG S6**, TIF file, 1.6 MB.

**FIG S7**, TIF file, 1.4 MB.

**FIG S8**, TIF file, 2.3 MB.

## ACKNOWLEDGMENTS

We thank all the participants in this study. We thank the all the clinical staff who made sample collection possible. In addition, we appreciate the MGH ED Cohort Sample Collection Team (team members listed as follows) for their efforts in collecting and processing these precious clinical samples: Nicole C. Charland, Anna L. K. Gonye, Irena Gushterova, Hargun K. Khanna, Thomas J. LaSalle, Kendall M. Lavin-Parsons, Brendan M. Lilley, Carl L. Lodenstein, Kasidet Manakongtreecheep, Justin D. Margolin, Brenna N. McKaig, Blair A. Parry, Maricarmen Rojas-Lopez, Brian C. Russo, Nihaarika Sharma, Jessica Tantivitt, Molly F. Thomas.

Direct funding for this project was provided in part by a grant or support from Mark, Lisa, and Enid Schwartz (to J.Z.L. and G.A.), a SAMANA Kay MGH Research Scholarship,

Nancy Zimmerman, Bruce Walker, an anonymous donor (financial support), Terry and Susan Ragon (G.A.), an American Lung Association COVID-19 Action Initiative grant (M.B.G.), grants from the Executive Committee on Research at MGH (M.B.G. and M.F.). N.H. was also funded by a gift from Arthur, Sandra, and Sarah Irving for the David P. Ryan, MD, Endowed Chair in Cancer Research. M.G. is the recipient of an EMBO long-term fellowship (ALTF 486-2018) and is a Cancer Research Institute/Bristol-Myers Squibb Fellow (CRI2993). This work was also supported by NIH grants (U01CA260476, U19 AI35995, R37AI80289, R01AI146785), by the Harvard Catalyst/Harvard Clinical and Translational Science Center (National Center for Advancing Translational Sciences, National Institutes of Health awards UL1 TR 001102 and UL1 TR 002541-01), and by the Harvard University Center for AIDS Research (NIAID 5P30AI060354).

We are also very grateful for the generous contributions of Olink Proteomics, Inc., and Novartis (in collaboration with SomaLogic, Inc.) for providing in-kind all proteomics assays presented in this work and for Radoslaw P. Nowak and Eric S. Fischer from Harvard Medical School and Aaron Schmidt from Ragon Institute of MGH, MIT, and Harvard, Cambridge, MA, USA, for providing SARS-CoV-2 spike, nucleocapsid, and RBD proteins, without which our findings would not have been possible.

Conceptualization: J.Z.L., G.A., Y.L., P.K., C.W., K.B. Establishment of the MGH ED cohort: M.F., M.S.-F., N.H., M.B.G. Resources: M.F., N.H., M.B.G. SARS-CoV-2 viral load assay: Y.L., J.R., J.P.F. Luminex and functional assays: P.K., S.F. Neutralization assay: M.G. Formal analysis: C.W., Y.L. Writing—original draft: Y.L. Writing—review and editing: J.Z.L., G.A., C.W., P.K., K.B., B.A.P., M.F., N.H., M.B.G., J.R., J.P.F.

There are no reported conflicts of interest related to this study.

## REFERENCES

- Li Y, Schneider AM, Mehta A, Sade-Feldman M, Kays KR, Gentili M, Charland NC, Gonye AL, Khanna HK, LaSalle TJ, Lavin-Parsons KM, Lilley BM, Lodenstein CL, Manakongtreecheep K, Margolin JD, McKaig BN, Parry BA, Rojas-Lopez M, Russo BC, Sharma N, Tantivit J, Thomas MF, Regan J, Flynn JP, Villani A-C, Hacoohen N, Goldberg MB, Filbin MR, Li JZ. 2021. SARS-CoV-2 viremia is associated with distinct proteomic pathways and predicts COVID-19 outcomes. *J Clin Invest* 131:e148635. <https://doi.org/10.1172/JCI148635>.
- Chen X, Zhao B, Qu Y, Chen Y, Xiong J, Feng Y, Men D, Huang Q, Liu Y, Yang B, Ding J, Li F. 2020. Detectable serum severe acute respiratory syndrome coronavirus 2 viral load (RNAemia) is closely correlated with drastically elevated interleukin 6 level in critically ill patients with coronavirus disease 2019. *Clin Infect Dis* 71:1937–1942. <https://doi.org/10.1093/cid/ciaa449>.
- Fajnzylber J, Regan J, Coxen K, Corry H, Wong C, Rosenthal A, Worrall D, Giguel F, Piechocka-Trocha A, Atyeo C, Fischinger S, Chan A, Flaherty KT, Hall K, Dougan M, Ryan ET, Gillespie E, Chishti R, Li Y, Jilg N, Hanidzari D, Baron RM, Baden L, Tsibris AM, Armstrong KA, Kuritzkes DR, Alter G, Walker BD, Yu X, Li JZ, Massachusetts Consortium for Pathogen Readiness. 2020. SARS-CoV-2 viral load is associated with increased disease severity and mortality. *Nat Commun* 11:5493. <https://doi.org/10.1038/s41467-020-19057-5>.
- Choi B, Choudhary MC, Regan J, Sparks JA, Padera RF, Qiu X, Solomon IH, Kuo H-H, Boucau J, Bowman K, Adhikari UD, Winkler ML, Mueller AA, Hsu TY-T, Desjardins M, Baden LR, Chan BT, Walker BD, Lichterfeld M, Brigl M, Kwon DS, Kanjilal S, Richardson ET, Jonsson AH, Alter G, Barczak AK, Hanage WP, Yu XG, Gaiha GD, Seaman MS, Cernadas M, Li JZ. 2020. Persistence and evolution of SARS-CoV-2 in an immunocompromised host. *N Engl J Med* 383:2291–2293. <https://doi.org/10.1056/NEJMc2031364>.
- Nabel KG, Clark SA, Shankar S, Pan J, Clark LE, Yang P, Coscia A, McKay LG, Varnum HH, Brusica V, Tolan NV, Zhou G, Desjardins M, Turbett SE, Kanjilal S, Sherman AC, Dighe A, LaRocque RC, Ryan ET, Tylek C, Cohen-Solal JF, Darcy AT, Tavella D, Clabbers A, Fan Y, Griffiths A, Correia IR, Seagal J, Baden LR, Charles RC, Abraham J. 2022. Structural basis for continued antibody evasion by the SARS-CoV-2 receptor binding domain. *Science* 375:eabl6251. <https://doi.org/10.1126/science.abc6251>.
- Cully M. 2022. A tale of two antiviral targets: and the COVID-19 drugs that bind them. *Nat Rev Drug Discov* 21:3–5. <https://doi.org/10.1038/d41573-021-00202-8>.
- Horby PW, Mafham M, Peto L, Campbell M, Pessoa-Amorim G, Spata E, Staplin N, Emberson JR, Prudon B, Hine P, Brown T, Green AC, Sarkar R, Desai P, Yates B, Bewick T, Tiberi S, Felton T, Baillie JK, Buch MH, Chappell LC, Day JN, Faust SN, Jaki T, Jeffery K, Juszcak E, Lim WS, Montgomery A, Mumford A, Rowan K, Thwaites G, Weinreich DM, Haynes R, Landray MJ, RECOVERY Collaborative Group. 2021. Casirivimab and imdevimab in patients admitted to hospital with COVID-19 (RECOVERY): a randomised, controlled, open-label, platform trial. *medRxiv* <https://doi.org/10.1101/2021.06.15.21258542>.
- Lundgren JD, Grund B, Barkauskas CE, Holland TL, Gottlieb RL, Sandkovsky U, Brown SM, Knowlton KU, Self WH, Files DC, Jain MK, Benfield T, Bowdish ME, Leshnowar BG, Baker JV, Jensen J-U, Gardner EM, Ginde AA, Harris ES, Johansen IS, Markowitz N, Matthay MA, Østergaard L, Chang CC, Davey VJ, Goodman A, Higgs ES, Murray DD, Murray TA, Paredes R, Parmar MKB, Phillips AN, Reilly C, Sharma S, Dewar RL, Teitelbaum M, Wentworth D, Cao H, Klekotka P, Babiker AG, Gelijns AC, Kan VL, Polizzotto MN, Thompson BT, Lane HC, Neaton JD, ACTIV-3/TICO LY-CoV555 Study Group. 2021. A neutralizing monoclonal antibody for hospitalized patients with Covid-19. *N Engl J Med* 384:905–914. <https://doi.org/10.1056/NEJMoa2033130>.
- Lucas C, Klein J, Sundaram ME, Liu F, Wong P, Silva J, Mao T, Oh JE, Mohanty S, Huang J, Tokuyama M, Lu P, Venkataraman A, Park A, Israelow B, Vogels CBF, Muenker MC, Chang C-H, Casanovas-Massana A, Moore AJ, Zell J, Fournier JB, Wyllie AL, Campbell M, Lee AI, Chun HJ, Grubaugh ND, Schulz WL, Farhadian S, Dela Cruz C, Ring AM, Shaw AC, Wisniewski AV, Yildirim I, Ko AI, Omer SB, Iwasaki A, Yale IMPACT Research Team. 2021. Delayed production of neutralizing antibodies correlates with fatal COVID-19. *Nat Med* 27:1178–1186. <https://doi.org/10.1038/s41591-021-01355-0>.
- Prévost J, Gasser R, Beaudoin-Bussièrès G, Richard J, Duerr R, Laumaea A, Anand SP, Goyette G, Benlarbi M, Ding S, Medjahed H, Lewin A, Perreault J, Tremblay T, Gendron-Lepage G, Gauthier N, Carrier M, Marcoux D, Piché A, Lavoie M, Benoit A, Loungnarath V, Brochu G, Haddad E, Stacey HD, Miller MS, Desforges M, Talbot PJ, Maule GTG, Côté M, Therrien C, Serhir B, Bazin R, Roger M, Finzi A. 2020. Cross-sectional evaluation of humoral responses against SARS-CoV-2 spike. *Cell Rep Med* 1:100126. <https://doi.org/10.1016/j.xcrm.2020.100126>.
- Weinreich DM, Sivapalasingam S, Norton T, Ali S, Gao H, Bhore R, Musser BJ, Soo Y, Rofail D, Im J, Perry C, Pan C, Hosain R, Mahmood A, Davis JD, Turner KC, Hooper AT, Hamilton JD, Baum A, Kyratsous CA, Kim Y, Cook A, Kampman W, Kohli A, Sachdeva Y, Graber X, Kowal B, DiCiccio T, Stahl N, Lipsich L, Braunstein N, Herman G, Yancopoulos GD, Trial Investigators. 2021. REGN-

- COVID, a neutralizing antibody cocktail, in outpatients with Covid-19. *N Engl J Med* 384:238–251. <https://doi.org/10.1056/NEJMoa2035002>.
12. Zohar T, Loos C, Fischinger S, Atyeo C, Wang C, Slein MD, Burke J, Yu J, Feldman J, Hauser BM, Caradonna T, Schmidt AG, Cai Y, Streeck H, Ryan ET, Barouch DH, Charles RC, Lauffenburger DA, Alter G. 2020. Compromised humoral functional evolution tracks with SARS-CoV-2 mortality. *Cell* 183: 1508–1519.e1512. <https://doi.org/10.1016/j.cell.2020.10.052>.
  13. Filbin MR, Mehta A, Schneider AM, Kays KR, Guess JR, Gentili M, Fenyves BG, Charland NC, Gonye ALK, Gushterova I, Khanna HK, LaSalle TJ, Lavin-Parsons KM, Lilley BM, Lodenstein CL, Manakongtreecheep K, Margolin JD, McKaig BN, Rojas-Lopez M, Russo BC, Sharma N, Tantivit J, Thomas MF, Gerszten RE, Heimberg GS, Hoover PJ, Lieb DJ, Lin B, Ngo D, Pelka K, Reyes M, Smillie CS, Waghay A, Wood TE, Zajac AS, Jennings LL, Grundberg I, Bhattacharyya RP, Parry BA, Villani A-C, Sade-Feldman M, Hacohen N, Goldberg MB. 2021. Longitudinal proteomic analysis of severe COVID-19 reveals survival-associated signatures, tissue-specific cell death, and cell-cell interactions. *Cell Rep Med* 2:100287. <https://doi.org/10.1016/j.xcrm.2021.100287>.
  14. Lv J, Hua Y, Wang D, Liu A, An J, Li A, Wang Y, Wang X, Jia N, Jiang Q. 2014. Kinetics of pulmonary immune cells, antibody responses and their correlations with the viral clearance of influenza A fatal infection in mice. *Virology* 11:57. <https://doi.org/10.1186/1743-422X-11-57>.
  15. Olchanski N, Hansen RN, Pope E, D'Cruz B, Fergie J, Goldstein M, Krilov LR, McLaurin KK, Nabrit-Stephens B, Oster G, Schaefer K, Shaya FT, Neumann PJ, Sullivan SD. 2018. Palivizumab prophylaxis for respiratory syncytial virus: examining the evidence around value. *Open Forum Infect Dis* 5:ofy031. <https://doi.org/10.1093/ofid/ofy031>.
  16. Mulangu S, Dodd LE, Davey RT, Tshiani Mbaya O, Proschan M, Mukadi D, Lusakibanza Manzo M, Nzolo D, Tshomba Oloma A, Ibanda A, Ali R, Coulibaly S, Levine AC, Grais R, Diaz J, Lane HC, Muyembe-Tamfum J-J, Sivahera B, Camara M, Kojan R, Walker R, Digheero-Kemp B, Cao H, Mukumbayi P, Mbala-Kingebeni P, Ahuka S, Albert S, Bonnett Z, Crozier I, Duvenhage M, Proffitt C, Teitelbaum M, Moench T, Aboulhab J, Barrett K, Cahill K, Cone K, Eckes R, Hensley L, Herpin B, Higgs E, Ledgerwood J, Pierson J, Smolskis M, Sow Y, Tierney J, Sivapalasingam S, Holman W, Gettinger N, Vallée D, Jr, PALM Consortium Study Team, et al. 2019. A randomized, controlled trial of Ebola virus disease therapeutics. *N Engl J Med* 381:2293–2303. <https://doi.org/10.1056/NEJMoa1910993>.
  17. Gaudinski MR, Berkowitz NM, Idris AH, Coates EE, Holman LA, Mendoza F, Gordon IJ, Plummer SH, Trofymenko O, Hu Z, Campos Chagas A, O'Connell S, Basappa M, Douek N, Narpala SR, Barry CR, Widge AT, Hicks R, Awan SF, Wu RL, Hickman S, Wycuff D, Stein JA, Case C, Evans BP, Carlton K, Gall JG, Vazquez S, Flach B, Chen GL, Francica JR, Flynn BJ, Kivalu NK, Capparelli EV, McDermott A, Masciola JR, Ledgerwood JE, Seder RA, VRC 612 Study Team. 2021. A monoclonal antibody for malaria prevention. *N Engl J Med* 385: 803–814. <https://doi.org/10.1056/NEJMoa2034031>.
  18. Lau KS, Juchheim AM, Cavaliere KR, Phillips SR, Lauffenburger DA, Haigis KM. 2011. In vivo systems analysis identifies spatial and temporal aspects of the modulation of TNF- $\alpha$ -induced apoptosis and proliferation by MAPKs. *Sci Signal* 4:ra16.
  19. RECOVERY Collaborative Group. 2021. Convalescent plasma in patients admitted to hospital with COVID-19 (RECOVERY): a randomised controlled, open-label, platform trial. *Lancet* 397:2049–2059. [https://doi.org/10.1016/S0140-6736\(21\)00897-7](https://doi.org/10.1016/S0140-6736(21)00897-7).
  20. Estcourt LJ, Turgeon AF, McQuilten ZK, McVerry BJ, Al-Beidh F, Annane D, Arabi YM, Arnold DM, Beane A, Bégin P, van Bentum-Puijk W, Berry LR, Bhimani Z, Birchall JE, Bonten MJM, Bradbury CA, Brunkhorst FM, Buxton M, Callum JL, Chassé M, Cheng AC, Cove ME, Daly J, Derde L, Detry MA, De Jong M, Evans A, Fergusson DA, Fish M, Fitzgerald M, Foley C, Goossens H, Gordon AC, Gosbell IB, Green C, Haniffa R, Harvala H, Higgins AM, Hills TE, Hoad VC, Horvat C, Huang DT, Hudson CL, Ichihara N, Laing E, Lamikanra AA, Lamontagne F, Lawler PR, Linstrum K, Litton E, Writing Committee for the REMAP-CAP Investigators, et al. 2021. Effect of convalescent plasma on organ support-free days in critically ill patients with COVID-19: a randomized clinical trial. *JAMA* 326:1690–1702. <https://doi.org/10.1001/jama.2021.18178>.
  21. Bégin P, Callum J, Jamula E, Cook R, Heddle NM, Tinmouth A, Zeller MP, Beaudoin-Bussièrès G, Amorim L, Bazin R, Loftsgard KC, Carl R, Chassé M, Cushing MM, Daneman N, Devine DV, Dumaresq J, Fergusson DA, Gabe C, Glesby MJ, Li N, Liu Y, McGeer A, Roubaille N, Sachais BS, Scales DC, Schwartz L, Shehata N, Turgeon AF, Wood H, Zarychanski R, Finzi A, Marceau D, Huang A, Carr H, Lin Y, Lall R, Graham C, Arsenault C, Sales V, Sidhu D, Semret M, Hamm C, Arhanchiague E, Solh Z, Srour N, Soliman K, Yee C, Laroche V, Nahiriak S, the CONCOR-1 Study Group, et al. 2021. Convalescent plasma for hospitalized patients with COVID-19: an open-label, randomized controlled trial. *Nat Med* 27:2012–2024. <https://doi.org/10.1038/s41591-021-01488-2>.
  22. Hagman K, Hedenstierna M, Gille-Johnson P, Hammam B, Grabbe M, Dillner J, Ursing J. 2020. Severe acute respiratory syndrome coronavirus 2 RNA in serum as predictor of severe outcome in coronavirus disease 2019: a retrospective cohort study. *Clin Infect Dis* 73:e2995–e3001. <https://doi.org/10.1093/cid/ciaa1285>.
  23. Jacobs JL, Bain W, Naqvi A, Staines B, Castanha PMS, Yang H, Boltz VF, Barratt-Boyes S, Marques ETA, Mitchell BL, Methé B, Olonisakin TF, Haidar G, Burke TW, Petzold E, Denny T, Woods CW, McVerry BJ, Lee JS, Watkins SC, St Croix CM, Morris A, Kearney MF, Ladinsky MS, Bjorkman PJ, Kitsios GD, Mellors JW. 2021. Severe acute respiratory syndrome coronavirus 2 viremia is associated with coronavirus disease 2019 severity and predicts clinical outcomes. *Clin Infect Dis* 74:1525–1533. <https://doi.org/10.1093/cid/ciab686>.
  24. Leisman D, Mehta A, Hacohen N, Filbin MR, Goldberg MB, MGH COVID-19 Collection & Processing Team. 2021. Trajectories of pulmonary epithelial and endothelial injury markers in COVID-19 patients requiring respiratory support at presentation. Abstract A1061. [https://doi.org/10.1164/ajrcm-conference.2021.203.1\\_MeetingAbstracts.A1061](https://doi.org/10.1164/ajrcm-conference.2021.203.1_MeetingAbstracts.A1061).
  25. Hensley MK, Bain WG, Jacobs J, Nambulli S, Parikh U, Cillo A, Staines B, Heaps A, Sobolewski MD, Rennick LJ, Macatangay BJC, Klamar-Blain C, Kitsios GD, Methé B, Somasundaram A, Bruno TC, Cardello C, Shan F, Workman C, Ray P, Ray A, Lee J, Sethi R, Schwarzmann WE, Ladinsky MS, Bjorkman PJ, Vignali DA, Duprex WP, Agha ME, Mellors JW, McCormick KD, Morris A, Haidar G. 2021. Intractable coronavirus disease 2019 (COVID-19) and prolonged severe acute respiratory syndrome coronavirus 2 (SARS-CoV-2) replication in a chimeric antigen receptor-modified T-cell therapy recipient: a case study. *Clin Infect Dis* 73:e815–e821. <https://doi.org/10.1093/cid/ciab072>.
  26. Brunet-Ratnasingham E, Anand SP, Gantner P, Dyachenko A, Moquin-Beaudry G, Brassard N, Beaudoin-Bussièrès G, Pagliuzza A, Gasser R, Benlarbi M, Point F, Prévost J, Laumaea A, Niessi J, Nayrac M, Sannier G, Orban C, Messier-Peet M, Butler-Laporte G, Morrison DR, Zhou S, Nakanishi T, Boutin M, Descôteaux-Dinelle J, Gendron-Lepage G, Goyette G, Bourassa C, Medjahed H, Laurent L, Rébillard R-M, Richard J, Dubé M, Fromentin R, Arbour N, Prat A, Laroche C, Durand M, Richards JB, Chassé M, Tétreault M, Chomont N, Finzi A, Kaufmann DE. 2021. Integrated immunovirological profiling validates plasma SARS-CoV-2 RNA as an early predictor of COVID-19 mortality. *Sci Adv* 7:eabj5629. <https://doi.org/10.1126/sciadv.abj5629>.
  27. Hagman K, Hedenstierna M, Rudling J, Gille-Johnson P, Hammam B, Grabbe M, Jakobsson J, Dillner J, Ursing J. 2022. Duration of SARS-CoV-2 viremia and its correlation to mortality and inflammatory parameters in patients hospitalized for COVID-19: a cohort study. *Diagn Microbiol Infect Dis* 102:115595. <https://doi.org/10.1016/j.diagmicrobio.2021.115595>.
  28. Kaneko N, Kuo H-H, Boucau J, Farmer JR, Allard-Chamard H, Mahajan VS, Piechocka-Trocha A, Lefteri K, Osborn M, Bals J, Bartsch YC, Bonheur N, Caradonna TM, Chevalier J, Chowdhury F, Diefenbach TJ, Einkauf K, Fallon J, Feldman J, Finn KK, Garcia-Broncano P, Hartana CA, Hauser BM, Jiang C, Kaplonek P, Karpell M, Koscher EC, Lian X, Liu H, Liu J, Ly NL, Michell AR, Rassadkina Y, Seiger K, Sessa L, Shin S, Singh N, Sun W, Sun X, Tichell HJ, Waring MT, Zhu AL, Alter G, Li JZ, Lingwood D, Schmidt AG, Lichtenfeld M, Walker BD, Yu XG, Padera RF, Massachusetts Consortium on Pathogen Readiness Specimen Working Group, et al. 2020. Loss of Bcl-6-expressing T follicular helper cells and germinal centers in COVID-19. *Cell* 183: 143–157.e113. <https://doi.org/10.1016/j.cell.2020.08.025>.
  29. Sullivan DJ, Gebo KA, Shoham S, Bloch EM, Lau B, Shenoy AG, Mosnaim GS, Gniadek TJ, Fukuta Y, Patel B, Heath SL, Levine AC, Meisenberg BR, Spivak ES, Anjan S, Huaman MA, Blair JE, Currier JS, Paxton JH, Gerber JM, Petrini JR, Broderick PB, Rausch W, Cordisco M-E, Hammel J, Greenblatt B, Cluzet VC, Cruser D, Oei K, Abinante M, Hammit LL, Sutcliffe CG, Forthall DN, Zand MS, Cachay ER, Raval JS, Kassaye SG, Foster EC, Roth M, Marshall CE, Yarava A, Lane K, McBee NA, Gawad AL, Karlen N, Singh A, Ford DE, Jabs DA, Appel LJ, Shade DM, et al. 2022. Early outpatient treatment for covid-19 with convalescent plasma. *N Engl J Med* 386:1700–1711. <https://doi.org/10.1056/NEJMoa2119657>.
  30. Richardson SI, Moore PL. 2021. Targeting Fc effector function in vaccine design. *Expert Opin Ther Targets* 25:467–477. <https://doi.org/10.1080/14728222.2021.1907343>.
  31. Suryadevara N, Shrihari S, Gilchuk P, VanBlargan LA, Binshtein E, Zost SJ, Nargi RS, Sutton RE, Winkler ES, Chen EC, Fouch ME, Davidson E, Doranz BJ, Chen RE, Shi P-Y, Carnahan RH, Thackray LB, Diamond MS, Crowe JE. 2021. Neutralizing and protective human monoclonal antibodies



- recognizing the N-terminal domain of the SARS-CoV-2 spike protein. *Cell* 184:2316–2331.e2315. <https://doi.org/10.1016/j.cell.2021.03.029>.
32. Yamin R, Jones AT, Hoffmann H-H, Schäfer A, Kao KS, Francis RL, Sheahan TP, Baric RS, Rice CM, Ravetch JV, Bournazos S. 2021. Fc-engineered antibody therapeutics with improved anti-SARS-CoV-2 efficacy. *Nature* 599:465–470. <https://doi.org/10.1038/s41586-021-04017-w>.
  33. Ullah I, Prévost J, Ladinsky MS, Stone H, Lu M, Anand SP, Beaudoin-Bussièrès G, Symmes K, Benlarbi M, Ding S, Gasser R, Fink C, Chen Y, Tauzin A, Goyette G, Bourassa C, Medjahed H, Mack M, Chung K, Wilen CB, Dekaban GA, Dikeakos JD, Bruce EA, Kaufmann DE, Stamatatos L, McGuire AT, Richard J, Pazgier M, Bjorkman PJ, Mothes W, Finzi A, Kumar P, Uchil PD. 2021. Live imaging of SARS-CoV-2 infection in mice reveals that neutralizing antibodies require Fc function for optimal efficacy. *Immunity* 54:2143–2158.e2115. <https://doi.org/10.1016/j.immuni.2021.08.015>.
  34. Yu KKQ, Fischinger S, Smith MT, Atyeo C, Cizmeci D, Wolf CR, Layton ED, Logue JK, Aguilar MS, Shuey K, Loos C, Yu J, Franko N, Choi RY, Wald A, Barouch DH, Koelle DM, Lauffenburger D, Chu HY, Alter G, Seshadri C. 2021. Comorbid illnesses are associated with altered adaptive immune responses to SARS-CoV-2. *JCI Insight* 6:146242. <https://doi.org/10.1172/jci.insight.146242>.
  35. Sette A, Crotty S. 2021. Adaptive immunity to SARS-CoV-2 and COVID-19. *Cell* 184:861–880. <https://doi.org/10.1016/j.cell.2021.01.007>.
  36. Wilhelm A, Widera M, Grikscheit K, Toptan T, Schenk B, Pallas C, Metzler M, Kohmer M, Hoehl S, Helfritz FA, Wolf T, Goetsch U, Ciesek S. 2021. Reduced neutralization of SARS-CoV-2 Omicron variant by vaccine sera and monoclonal antibodies. *medRxiv* <https://doi.org/10.1101/2021.12.07.21267432>.
  37. Cao YR, Wang J, Jian F, Xiao T, Song W, Yisimayi A, Huang W, Li Q, Wang P, An R, Wang J, Wang Y, Niu X, Yang S, Liang H, Sun H, Li T, Yu Y, Cui Q, Liu S, Yang X, Du S, Zhang Z, Hao X, Shao F, Jin R, Wang X, Xiao J, Wang Y, Xie XS. 2021. B.1.1.529 escapes the majority of SARS-CoV-2 neutralizing antibodies of diverse epitopes. *bioRxiv* <https://doi.org/10.1038/s41586-021-04385-3>.
  38. Fischinger S, Fallon JK, Michell AR, Broge T, Suscovich TJ, Streeck H, Alter G. 2019. A high-throughput, bead-based, antigen-specific assay to assess the ability of antibodies to induce complement activation. *J Immunol Methods* 473:112630. <https://doi.org/10.1016/j.jim.2019.07.002>.
  39. Akaike H, Petrov BN, Csaki F. 1973. Second international symposium on information theory. Akadémiai Kiadó, Budapest, Hungary.
  40. Atyeo C, Fischinger S, Zohar T, Slein MD, Burke J, Loos C, McCulloch DJ, Newman KL, Wolf C, Yu J, Shuey K, Feldman J, Hauser BM, Caradonna T, Schmidt AG, Suscovich TJ, Linde C, Cai Y, Barouch D, Ryan ET, Charles RC, Lauffenburger D, Chu H, Alter G. 2020. Distinct early serological signatures track with SARS-CoV-2 survival. *Immunity* 53:524–532.e524. <https://doi.org/10.1016/j.immuni.2020.07.020>.